Available online at www.sciencedirect.com

ScienceDirect

Geochimica et Cosmochimica Acta 203 (2017) 89–102

Geochimica et Cosmochimica Acta

www.elsevier.com/locate/gca

Iron isotopic compositions of adakitic and non-adakitic granitic magmas: Magma compositional control and subtle residual garnet effect

Yongsheng He [a,*], Hongjie Wu [a], Shan Ke [a], Sheng-Ao Liu [a], Qiang Wang [b,c]

[a] State Key Laboratory of Geological Processes and Mineral Resources, China University of Geosciences, Beijing 100083, China
[b] State Key Laboratory of Isotope Geochemistry, Guangzhou Institute of Geochemistry, Chinese Academy of Sciences, Guangzhou 510640, China
[c] CAS Center for Excellence in Tibetan Plateau Earth Sciences, China

Received 3 June 2016; accepted in revised form 6 January 2017; Available online 16 January 2017

Abstract

Here we present iron (Fe) isotopic compositions of 51 well-characterized adakitic and non-adakitic igneous rocks from the Dabie orogen, Central China and Panama/Costa Rica, Central America. Twelve I-type non-adakitic granitoid samples from the Dabie orogen yield $\delta^{56}Fe$ ranging from −0.015‰ to 0.184‰. The good correlations between $\delta^{56}Fe$ and indices of magma differentiation (e.g., SiO_2, FeOt, Mg#, and $Fe^{3+}/\Sigma Fe$) suggest Fe^{2+}-rich silicate and oxide minerals dominated fractional crystallization with $\Delta^{56}Fe_{melt\text{-}crystal} \sim 0.06‰$ may account for the $\delta^{56}Fe$ variation in these samples. One A-type granite sample from the Dabie orogen has $\delta^{56}Fe$ as high as 0.447‰, likely indicating less magnetite crystallization and an increase in $10^3 ln\beta_{melt}$ with magma (Na + K)/(Ca + Mg). Combined with the literature data, most high silica ($SiO_2 \geqslant 71$ wt.%) granitic rocks define a good positive linear correlation between $\delta^{56}Fe$ and (Na + K)/(Ca + Mg): $\delta^{56}Fe = 0.0062‰ \times (Na + K)/(Ca + Mg) + 0.130‰$ ($R^2 = 0.66$). Given that fractional crystallization also tends to increase $\delta^{56}Fe$ with (Na + K)/(Ca + Mg), this correlation can serve as the maximum estimate of the magma compositional control on Fe isotope fractionation. Low-Mg adakitic samples (LMA) have $\delta^{56}Fe$ ranging from 0.114‰ to 0.253‰. The melt compositional control on LMA $\delta^{56}Fe$ could be insignificant due to their limited (Na + K)/(Ca + Mg) variation. Except for one sample that may be affected by late differentiation, 14 out of 15 LMA have $\delta^{56}Fe$ increasing with $(Dy/Yb)_N$, reflecting a subtle but significant effect of residual garnet proportion. This serves as evidence for that source mineralogy may play an important role in fractionating Fe isotopes during partial melting. Dabie and Central America high-Mg adakitic samples have homogeneous Fe isotopic compositions with mean $\delta^{56}Fe$ of 0.098 ± 0.038‰ (2SD, $N = 11$) and 0.085 ± 0.045‰ (2SD, $N = 11$), respectively. These samples have undergone melt-mantle interaction, which may neutralize the possible $\delta^{56}Fe$ variation of their pristine magmas derived by partial melting of eclogitic rocks.

Keywords: Iron isotopic composition; Adakitic rocks; Melt compositional control; Residual garnet effect; Crustal recycling

1. INTRODUCTION

Significant iron (Fe) isotope fractionation (e.g., $\delta^{56}Fe > 0.5‰$, ten times larger than the analytical uncertainty) has been observed in terrestrial igneous rocks (e.g., Weyer and Ionov, 2007; Teng et al., 2008; Dauphas et al., 2009a; Williams and Bizimis, 2014; He et al., 2015b). It remains unclear to what extent these variations reflect magma processes or source composition (e.g., oxidation state, mineralogy, and compositions) (e.g., Dauphas et al., 2014; Williams and Bizimis, 2014; Zambardi et al., 2014;

* Corresponding author.
E-mail address: heys@cugb.edu.cn (Y. He).

http://dx.doi.org/10.1016/j.gca.2017.01.005
0016-7037/

Foden et al., 2015; Zhu et al., 2015a); in particular, whether Fe isotopes can help reveal redox conditions of planetary and igneous processes (Dauphas et al., 2014; Williams and Bizimis, 2014) or whether additional factors, such as co-ordination environment, play a significant role (Sossi and O'Neill, 2017). Fe has two oxidation states (ferrous Fe^{2+} and ferric Fe^{3+}) in terrestrial silicate phases. The mean force constant of Fe^{3+} bearing bonds is higher than that of Fe^{2+} bearing bonds in silicate glasses, which predicts an enrichment of heavy isotopes in the former and highlights the potential of Fe isotopes as a tracer of magma redox conditions (Dauphas et al., 2014). However, predicted isotope fractionation induced by the distribution of Fe^{3+} and Fe^{2+} during partial melting of mantle peridotite can only account for one-third of the observed difference between middle ocean ridge basalts (MORB) and the upper mantle (~0.1‰ on $\delta^{56}Fe$; Teng et al., 2013; Dauphas et al., 2014). In addition to the distribution of Fe^{3+} and Fe^{2+}, the difference in the coordination environment of Fe is a complementary but independent mechanism of Fe isotope fractionation (Sossi and O'Neill, 2017). Among Fe^{2+}-enriched silicate minerals, garnet with Fe^{2+} in VIII-coordination has a Fe isotopic composition substantially lower than coexisting olivine and pyroxenes, in which Fe^{2+} is mainly in VI-coordination (e.g., $\Delta^{56}Fe_{garnet\text{-}cpx}$ in eclogites down to −0.42‰ and on average ~ −0.26‰; Beard and Johnson, 2004; Williams et al., 2009). Accordingly, Fe isotope fractionation during partial melting might be also controlled by source mineralogy. Partial melting of garnet-rich sources (e.g., pyroxenite and recycled eclogite) may produce Fe isotope fractionation larger than peridotite melting and contribute to the high $\delta^{56}Fe$ end-member of ocean island basalts (Williams and Bizimis, 2014; Sossi and O'Neill, 2017). However, the relative importance of redox and coordination environment is complicated by source heterogeneity and Fe isotope fractionation during magma differentiation (Teng et al., 2008; Williams and Bizimis, 2014; Foden et al., 2015; Sossi and O'Neill, 2017). Observations serving as evidence to constrain to what extent source mineralogy can affect Fe isotope fractionation during partial melting, however, remain scarce.

Adakitic rocks may help to provide these constraints, as they are derived by partial melting of eclogitic rocks with variably abundant residual garnet (Defant and Drummond, 1990; Rapp and Watson, 1995; He et al., 2011), and thus may provide a test on the role of source mineralogy in fractionating Fe isotopes during partial melting processes. Eclogitic partial melting is referred to here as partial melting of basaltic sources at depths ⩾50 km with garnet and clinopyroxene as the only two dominant residual minerals, which occurs either during hot subduction of oceanic crust or at the base of thickened continental crust. Adakitic rocks can be identified by their high Sr/Y (⩾40), $(La/Yb)_N$ (⩾20) and low Y (⩽18 ppm) and Yb (⩽1.9 ppm) contents (Defant and Drummond, 1990; Castillo, 2006; Moyen, 2009). It should be noted that high Sr/Y magmas can be produced in other ways, e.g., fractional crystallization and derivation from high Sr/Y sources (Moyen, 2009). Phanerozoic adakitic rocks derived from eclogitic partial melting have been identified in a limited number of locations, e.g., those from the Central American Arc and the Dabie orogen (e.g., Abratis and Wörner, 2001; Wang et al., 2007; He et al., 2011). Most adakitic rocks have high Mg# (e.g.>50) as well as MgO, Cr and Ni contents at a given SiO_2 (so-called "high-Mg adakitic rocks" or "HMA"), and may have experienced intensive interaction with the upper mantle (Defant and Drummond, 1990; Rapp et al., 1999; Huang et al., 2008). Pristine partial melts derived from eclogitic rocks (e.g., low-Mg adakitic rocks derived from thickened lower continental crust; He et al., 2011) thus are the best candidate to test the role of source mineralogy in fractionating Fe isotopes. As yet, no high precision Fe isotopic data has been reported for any adakitic rocks.

Low-Mg adakitic rocks (LMA) generally have felsic compositions with SiO_2 up to >70 wt.% (Wang et al., 2007; He et al., 2011). Before the Fe isotope fractionation arising from partial melting can be quantified, the effects of magmatic differentiation must be considered. Previous studies have revealed that high silica granitic magmas with SiO_2 ⩾ 71 wt.% have $\delta^{56}Fe$ systematically higher than low silica magmas, which has been explained by fluid exsolution (Poitrasson and Freydier, 2005; Heimann et al., 2008), fractional crystallization (Schuessler et al., 2009; Sossi et al., 2012; Telus et al., 2012; Dauphas et al., 2014; Foden et al., 2015), and thermal and chemical diffusion (Zambardi et al., 2014; Zhu et al., 2015a). In addition, Dauphas et al. (2014) reveals that rhyolitic glasses with SiO_2 ~ 76% have Fe-O bonds stronger than those in basaltic to dacitic glasses (SiO_2 from 45% to 64%), which predicts a magma compositional control on Fe isotope fractionation. The relevant mechanism has not been well understood and may be controlled by the counteracting role of alkaline and alkaline-earth cations in stabilizing IV-coordinated Fe^{3+} (Schuessler et al., 2009; Dauphas et al., 2014; Foden et al., 2015).

In this study, we present the first Fe isotopic data for adakitic rocks, including 15 LMA and 22 HMA samples from the Dabie orogen (Central China) and Panama/Costa Rica (Central America), to constrain the source mineralogy effect on Fe isotope fractionation during partial melting. Thirteen non-adakitic granitoid samples from the Dabie orogen, with SiO_2 spanning from 56 to 77 wt.%, are also measured to better understand Fe isotope fractionation during differentiation of intermediate and felsic magmas and to constrain the extent of magma compositional control. Combined with the literature data, a good correlation between $\delta^{56}Fe$ and (Na + K)/(Ca + Mg) has been established for high silica (SiO_2 ⩾ 71 wt.%) granitic magmas, serving as the maximum estimate of magma compositional control on Fe isotope fractionation. LMA yield $\delta^{56}Fe$ increasing with $(Dy/Yb)_N$, reflecting the detectable role of residual garnet in fractionating Fe isotopes during eclogitic partial melting. HMA from both the Dabie orogen and Panama/Costa yield nearly homogeneous MORB-like $\delta^{56}Fe$, likely as a consequence of melt-mantle interaction.

2. SAMPLE DESCRIPTION

The samples investigated in this study include 39 Early Cretaceous granitoids from the Dabie orogen, Central

China (Fig. S1) and 11 adakites and 1 basaltic oceanic crust sample from Costa Rica and Panama, Central America (Fig. S2). Dabie adakitic rocks are related to delamination of lower continental crust, and adakites from Central America formed after ridge collision at the edge of a slab window, based on the local magmatic sequence and adakitic compositions from these occurrences matching with what is expected by experimental studies and trace element modelling (e.g., Rapp et al., 1999; Abratis and Wörner, 2001; Wang et al., 2007; Huang et al., 2008; Wegner et al., 2010; He et al., 2011). These samples measured here represent the scarce examples of Phanerozoic true adakitic rocks derived from eclogitic partial melting. Detailed petrology and geochemistry of our samples are found in Abratis and Wörner (2001), Wang et al. (2007), Liu et al. (2010), Wegner et al. (2010), He (2010) and He et al. (2011, 2013), and only a brief description relevant to this study will be given below. Geochemistry of the samples investigated here is summarized in Table S3.

2.1. Post-collisional adakitic and non-adakitic granitoids from the Dabie orogen

Dabie granitoids measured here are related to delamination of the lower continental crust and collapse of the pre-existing mountain keel beneath the orogen at ca. 130 Ma (Wang et al., 2007; Huang et al., 2008; He, 2010; He et al., 2011). Dabie low-Mg adakitic rocks (LMA) was emplaced during 143–130 Ma. These LMA generally have variably high and positively inter-correlated Sr/Y, $(La/Yb)_N$, $(Dy/Yb)_N$ and Nb/Ta ratios, indicating a derivation from mafic crust at depths > 50 km with garnet + pyroxene residua (He et al., 2011). Trace element modelling indicates a low degree of partial melting (ca. 5 %), and that gradually elevated $(Dy/Yb)_N$ corresponds to an increasing proportion of residual garnet (He et al., 2011). Liquidus experiments in equilibrium with garnet + pyroxene assemblage indicate partial melting likely occurred at $T \geqslant 1075$ °C and $P \geqslant 2.0$ GPa with the initial melt containing ~ 6 wt.% H_2O (Xiao and Clemens, 2007). Low-Mg features of Dabie LMA (e.g., Mg# < 50, Ni < 20 ppm) suggest that they may not have interacted with the upper mantle (Wang et al., 2007; He et al., 2011). High-Mg adakitic rocks (HMA) (132–131 Ma) occur in the eastern margin of the Dabie orogen and along the Tan-Lu fault (Fig. S1; Huang et al., 2008; He, 2010; Liu et al., 2010). It should be noted that 7 samples from Liu et al. (2010) locate in the eastern expanding zone of the orogen and will be also referred as Dabie HMA hereafter. Dabie HMA have SiO_2 ranging from 56 to 70 wt.%, Mg# up to 63, Ni contents up to 121 ppm, Sr/Y > 40, and Y < 18 ppm. They are interpreted as partial melts derived from delaminated and foundering lower continental crust and have suffered melt-mantle interaction enroute to crustal depths (Huang et al., 2008; Liu et al., 2010). Dabie adakitic granitoids consist of amphibole, biotite, two feldspars and quartz with accessory magnetite, sphene, zircon and apatite (e.g., Wang et al., 2007; Huang et al., 2008; He et al., 2011). Based on $Fe^{3+}/\Sigma Fe$, equilibrium at liquidus temperatures using Rhyolite-MELTS (Gualda et al., 2012) reveal magma oxygen fugacity ranging from QFM + 1.7 to QMF + 4.1, with the majority clustering between QFM + 2.0 ~ QFM + 3.0.

Dabie granitoids younger than 130 Ma show non-adakitic features (e.g. Wang et al., 2007; He et al., 2011). They are mainly I-type with A/CNK (Al/(Ca + Na + K) in mole ratio) < 1.1 and derived from shallow crust at depths < 40 km without residual garnet. Only one sample 06HSW-2 shows affinity to A-type granites (Fig. S3). Dabie non-adakitic granitoids contain a mineral assemblage similar to adakitic ones, except at some intermediate rocks (e.g., Fujinshan and Fushan) where clinopyroxene is identified (He et al., 2011). Magma oxygen fugacity of Dabie non-adakitic granitoids ranges from QFM + 2.0 to QFM + 3.9.

2.2. Cenozoic adakites from Costa Rica and Panama, Central American arc

Late Cenozoic adakites from Central America were collected from isolated, geographically scattered volcanic centers erupted in southern Costa Rica and west-central Panama over the past 3.5 Ma. These samples are characterized by intermediate to felsic compositions (SiO_2 = 54–71 wt.%), high Mg# up to 70, high Sr/Y up to 171, steep heavy rare earth element (REE) patterns, and Sr-Nd-Pb isotopic compositions similar to local oceanic basement (Abratis and Wörner, 2001; Wegner et al., 2010). These geochemical features demonstrate that Central America adakites were derived from partial melting of subducted oceanic crust as a consequence of subduction of the Cocos Ridge and slab-window formation beneath Central America (Abratis and Wörner, 2001; Wegner et al., 2010). It has been suggested, on the basis of their Mg# up to 70, that these magmas have experienced strong interaction with the mantle wedge enroute to the surface, as pristine melts derived from eclogitic rocks have Mg# ⩽ 50 (Fig. 1b; Rapp et al., 1999). $Fe^{3+}/\Sigma Fe$ data suggest magma oxygen fugacity ⩾QFM + 2.6. One basaltic sample (PAN-06-194, from Wegner et al., 2010) represents the Caribbean large igneous province (CLIP) basement as a reference for the melted oceanic rocks at the slab window edge (Wegner et al., 2010).

3. ANALYTICAL METHODS

Iron isotope analyses were conducted at the Isotope Geochemistry Laboratory, China University of Geosciences, Beijing. The chemistry procedures are largely after Dauphas et al. (2009b) and detailed in He et al. (2015a). Approximately 5–20 mg whole rock powders were dissolved in Teflon beakers in a mixture of HF-HNO_3-$HClO_4$, and then refluxed with aqua regia (HCl: HNO_3 = 3:1) and excess HNO_3 aqua regia (HCl: HNO_3 = 2:1) successively at 130 °C. The solutions were subsequently evaporated to dryness at 100 °C. Finally, residues were dissolved in 6 N HCl for chromatographic purification. Iron was separated from matrix elements and potential isobars with AG1X-8 resin (200–400 mesh) in a HCl medium. Whole procedure blank is ⩽10 ng and can be considered negligible, considering ⩾100 μg sample Fe was processed. Isotopic ratios were analyzed by the

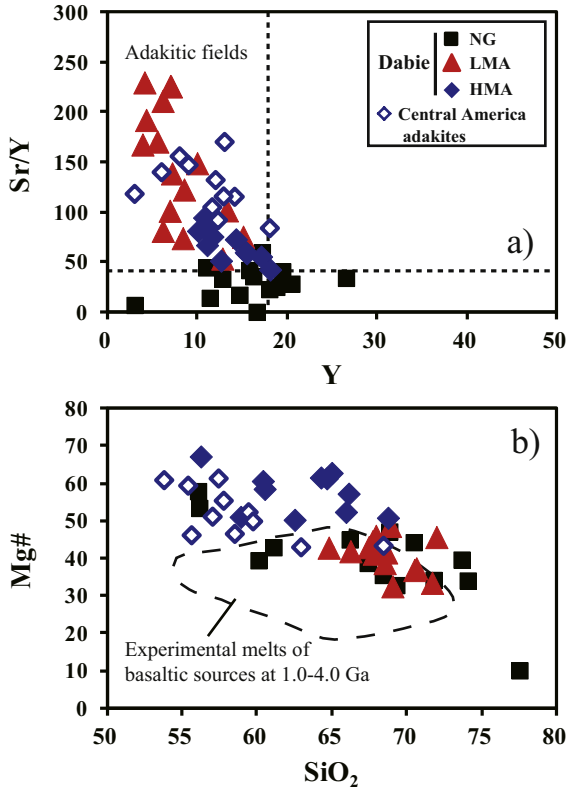

Fig. 1. Sr/Y vs Y and Mg# vs SiO_2 patterns. Adakitic field is defined by Sr/Y ⩾ 40 and Y ⩽ 18 ppm (Defant and Drummond, 1990). The field of experimental melts of basaltic sources at 1.0–4.0 GPa is after Rapp et al. (1999), and magmas that have Mg# higher than the experimental melts should have experienced melt-mantle interaction. NG, LMA, and HMA represent non-adakitic granitoids, low-Mg and high-Mg adakitic rocks from the Dabie orogen, respectively. Data for Dabie and Central America samples are from He (2010), He et al. (2011), Liu et al. (2010), Wang et al. (2007), Abratis and Wörner (2001) and Wegner et al. (2010).

sample-standard bracketing method using a Thermo-Finnigan Neptune Plus MC-ICPMS on high resolution modes. The isotopic measurement sequence was repeated nine times for each sample Fe solution to get better accuracy, and the data are reported in the traditional δ values relative to IRMM-014 ($\delta^{i}Fe = [(^{i}Fe/^{54}Fe)_{sample}/(^{i}Fe/^{54}Fe)_{IRMM\text{-}014} - 1] \times 1000$, where i can be 56 or 57). Two standard errors of the mean are reported after Dauphas et al. (2009b) and He et al. (2015a), with consideration of those arising both from chemical procedures and from the MC-ICPMS measurement. Based on totally > 300 duplicate measurements on 23 geological standards with different matrices, the long-term external reproducibility and accuracy on $\delta^{56}Fe$ are estimated to be better than ±0.03‰ (2SD) (He et al., 2015a). Geostandard JA-1, GSP-2 and GSR-1 were processed during the course of this study (Supplementary Table S1). The results agree well with previous studies (Poitrasson and Freydier, 2005; Craddock and Dauphas, 2010; Millet et al., 2012).

Only the total Fe_2O_3 contents have been previously reported for the Dabie samples (Liu et al., 2010; He et al., 2011). To quantify $Fe^{3+}/\Sigma Fe$, the FeO was determined by redox titration using $K_2Cr_2O_7$ solution for Dabie samples at China University of Geosciences, Beijing after (Yin and Li, 2011). Sample powders were decomposed with hot (close to boiling) concentrated HF and 1:1 H_2SO_4 for 10 min. The sample solutions were then complexed and buffered by newly boiled, cold boric acid. Ferrous Fe was then titrated by potassium dichromate with two sodium diphenylamine sulfonate as the indicator. Fe_2O_3 and $Fe^{3+}/\Sigma Fe$ were then calculated accordingly. Based on the result for BCR-2, GSP-2, and GSR-1 and duplicate analyses on three unknown samples (Table S2), $Fe^{3+}/\Sigma Fe$ reported here is accurate within ±10%.

4. RESULTS

Our Fe isotopic data are reported in Table 1 and shown in Fig. 2. All samples reported in this study largely follow the $\delta^{56}Fe$ vs SiO_2 trend defined by previously published global intermediate to felsic rocks (Fig. 2a) (Dauphas et al., 2009a; Poitrasson and Freydier, 2005; Heimann et al., 2008; Schuessler et al., 2009; Sossi et al., 2012; Telus et al., 2012; Zambardi et al., 2014; Foden et al., 2015).

Twelve I-type, non-adakitic granitoids from the Dabie orogen that have the most diverse major elemental compositions (e.g., SiO_2 from 56 to 74 wt.%) exhibit a $\delta^{56}Fe$ variation ranging from −0.015‰ to 0.184‰. One A-type granite sample (06HSW-2) with $SiO_2 \sim 76$ wt.% has $\delta^{56}Fe \sim 0.447$‰, higher than I-type, non-adakitic granitoids at a given FeOt. $\delta^{56}Fe$ of Dabie LMA (SiO_2: 65 ~ 72 wt.%) range from 0.114‰ to 0.253‰, while Dabie HMA have almost homogeneous Fe isotopic compositions with a mean $\delta^{56}Fe$ of 0.098 ± 0.038‰ (2SD, $N = 11$).

Adakites from Central America (SiO_2: 54–59 wt.%) also have homogeneous Fe isotopic compositions with a mean $\delta^{56}Fe$ of 0.080 ± 0.034‰ (2SD, $N = 10/11$), except for one high silica sample (PAN-05–047). PAN-05–047 with $SiO_2 = 68$ wt.% has a slightly higher $\delta^{56}Fe$ of 0.133‰. The one basaltic sample PAN-06–194, representing local oceanic crust basement (CLIP), has a $\delta^{56}Fe$ of 0.071‰, within the range of global MORB (0.105 ± 0.043‰, 2SD; Teng et al., 2013; and reference therein).

5. DISCUSSION

A large variation in $\delta^{56}Fe$ is observed in the Dabie non-adakitic granitoids and LMA. Good correlations between $\delta^{56}Fe$ and major elemental compositions can be identified for these samples, e.g., gradually higher $\delta^{56}Fe$ with increasing SiO_2 and decreasing FeOt (Fig. 2). Diffusion is not considered here since all Dabie samples are well crystallized and far away from the pluton boundary. The phenomenon that high silicic (SiO_2 ⩾ 71 wt.%) magmas generally yield $\delta^{56}Fe$ significant higher than low silicic (SiO_2 < 71 wt.%) ones was first noted by Poitrasson and Freydier (2005), and originally attributed to exsolution of low $\delta^{56}Fe$ ferrous chloride fluids at the late stage of magma differentiation (Poitrasson and Freydier, 2005; Heimann et al., 2008). Th/U ratio is used here as an index of fluid exsolution, as it typically does not fractionate significantly during magma

Table 1
Iron isotopic compositions of adakitic and non-adakitic granitoids from the Dabie orogen, Central China and adakites from Costa Rica and Panama, Central America.

Sample	SiO_2 (wt.%)	$Fe^{3+}/\Sigma Fe$ (%)	Mg#	(Na + K)/Al	(Na + K)/(Ca + Mg)	$(Dy/Yb)_N$	$\delta^{56}Fe$	2se	$\delta^{57}Fe$	2se	n
Dabie low-Mg adakitic granitoids											
06FJ-1	71.95	34	46	0.78	4.64	1.91	0.140	0.038	0.213	0.053	9
07EJ-2	68.50	56	39	0.79	4.17	1.91	0.148	0.038	0.218	0.053	9
07EJ-6	67.91	58	46	0.70	2.29	1.27	0.128	0.038	0.198	0.053	9
06LS-2	70.61	57	37	0.80	9.41	2.98	0.234	0.038	0.353	0.053	9
07LS-5	67.78	52	41	0.74	3.99	3.12	0.184	0.038	0.260	0.053	9
07DT-2	64.77	46	43	0.74	2.94	1.93	0.114	0.035	0.177	0.045	10
07DT-3	66.22	42	42	0.76	2.98	1.74	0.154	0.029	0.228	0.042	9
07ZB-1	67.69	39	45	0.78	4.08	3.00	0.144	0.037	0.227	0.048	9
07LD-1	68.86	40	49	0.75	3.36	1.44	0.140	0.037	0.206	0.048	9
EGB-1	70.48	43	37	0.66	2.52	1.22	0.121	0.037	0.193	0.048	9
EGB-2	69.02	38	33	0.77	4.72	1.54	0.141	0.037	0.235	0.048	9
EGB-7	71.66	47	33	0.81	6.12	1.38	0.248	0.048	0.344	0.068	9
Replicate							0.257	0.041	0.383	0.065	9
Weighted mean							0.253	0.031	0.364	0.047	
YFD-3	68.60	33	42	0.72	3.74	2.51	0.195	0.048	0.291	0.068	9
YFD-8	67.90	32	44	0.71	2.96	2.16	0.174	0.054	0.249	0.076	8
Replicate							0.157	0.041	0.232	0.065	9
Weighted mean							0.163	0.033	0.239	0.050	
YFD-9	67.44	31	43	0.71	3.23	2.13	0.139	0.054	0.216	0.076	8
Dabie high-Mg adakitic granitoids											
07GH-5	68.72	44	51	0.77	2.91	1.45	0.136	0.029	0.180	0.049	9
07MC-1	64.64	45	61	0.73	1.48	1.53	0.096	0.029	0.154	0.049	9
07MC-3	64.25	41	62	0.74	1.44	1.47	0.103	0.029	0.114	0.049	9
07MC-5	64.97	44	63	0.76	1.53	1.50	0.104	0.029	0.137	0.049	9
DMC-1	58.90	34	51	0.67	1.20	1.72	0.074	0.031	0.109	0.045	9
DMC-5	62.50	37	50	0.74	1.58	1.66	0.076	0.031	0.111	0.045	9
XLZ-1	65.92	44	52	0.73	1.82	1.23	0.097	0.031	0.122	0.045	9
XLZ-4	66.10	45	57	0.72	1.84	1.39	0.123	0.031	0.218	0.045	9
FJZ-1	60.38	38	61	0.69	0.95	1.45	0.099	0.038	0.134	0.053	9
FJZ-4	60.50	35	59	0.69	1.01	1.50	0.089	0.038	0.120	0.053	9
QTJ-2	56.24	40	67	0.74	0.99	1.70	0.077	0.038	0.123	0.053	9
Dabie non-adakitic granitoids											
06FJS-2	56.14	37	53	0.53	0.68	1.31	-0.015	0.054	-0.009	0.076	8
07FJS-2	56.06	31	58	0.55	0.59	1.25	0.024	0.051	0.010	0.072	9
06FS-1	68.81	43	47	0.75	3.03		0.061	0.051	0.102	0.072	9
06FS-4	70.44	53	44	0.76	3.18	1.17	0.122	0.051	0.178	0.072	9
06TG-1	61.09	46	43	0.61	1.88	1.60	0.095	0.029	0.128	0.042	9
06TG-2	60.09	53	39	0.62	1.60	1.43	0.094	0.029	0.164	0.042	9
06ZY-2	66.17	50	45	0.71	2.23	1.04	0.099	0.029	0.154	0.042	9
06XT-1	73.63	51	40	0.80	6.30	0.94	0.178	0.029	0.259	0.042	9
07SJS-2	74.04	57	34	0.77	5.49	1.09	0.184	0.023	0.263	0.040	9
07YC-1	71.76	48	34	0.78	5.04	1.75	0.139	0.023	0.229	0.040	9
07YC-3	69.28	68	33	0.81	6.09	1.59	0.153	0.023	0.240	0.040	9
07XM-3	68.38	43	36	0.74	4.05	1.64	0.143	0.023	0.211	0.040	9
06HSW-2	77.49	48	10	0.95	53.08	0.74	0.447	0.029	0.660	0.042	9

(*continued on next page*)

Table 1 (*continued*)

Sample	SiO_2 (wt.%)	$Fe^{3+}/\Sigma Fe$ (%)	Mg#	(Na + K)/Al	(Na + K)/(Ca + Mg)	$(Dy/Yb)_N$	$\delta^{56}Fe$	2se	$\delta^{57}Fe$	2se	n
Adakites from Costa Rica and Panama, Central America											
PAN-05-047	68.40		43	0.67	2.65	1.50	0.133	0.032	0.189	0.050	9
PAN-06-043	62.90		43	0.44	1.98	2.53	0.108	0.019	0.148	0.039	9
PAN-06-006	59.40		52	0.53	0.90	1.75	0.085	0.032	0.081	0.050	9
PAN-06-014	55.60		46	0.44	0.70	1.72	0.063	0.032	0.091	0.050	9
PAN-06-165	59.70		50	0.52	0.87	1.68	0.064	0.019	0.082	0.039	9
PAN-06-177	57.00		51	0.48	0.77	1.68	0.065	0.019	0.104	0.039	9
ALT-58	57.40	50	61	0.50	0.63	1.60	0.075	0.019	0.101	0.039	9
ALT-60	53.77	38	61	0.45	0.48	1.58	0.108	0.019	0.161	0.039	9
ALT-63	57.74	66	55	0.51	0.74	1.85	0.082	0.019	0.116	0.039	9
VIT-54	55.37	74	60	0.50	0.58	1.70	0.082	0.019	0.113	0.039	9
VIT-55	58.48	79	47	0.50	0.97	1.95	0.067	0.016	0.093	0.036	9
Basalt from the Caribbeab large igneous province basement											
PAN-06-194	48.10		59	0.35	0.24	1.11	0.071	0.019	0.112	0.039	9

Notes: Elemental data are from Abratis and Wörner (2001), He (2010), He et al. (2011), Huang et al. (2008), Liu et al. (2010), Wang et al. (2007), and Wegner et al. (2010). $Fe^{3+}/\Sigma Fe$ for Dabie samples are calculated based on ferrous Fe contents determined by redox titration here as well as total Fe contents previously reported. (Na + K)/Al and (Na + K)/(Ca + Ma) are mole ratios.

processes, but may be changed during fluid exsolution due to the higher fluid mobility of U than Th (Hawkesworth et al., 1997; Bali et al., 2009; Ling et al., 2011). As shown in Fig. 3, most Dabie non-adakitic granitoids and LMA have Th/U around the mean lower continental crust (LCC ~ 5.9, Rudnick and Gao, 2003), except few LMA samples from Egongbao and Yunfengding that yield Th/U up to 51 by depletion of U. Zircon from Egongbao and Yunfengding samples, however, has a mean Th/U from 0.10 to 0.27 (Wang et al., 2007), lower than those of other plutons (Liangshan ~ 0.80, Shangcheng ~ 1.35, Fujinshan ~ 1.59, Fushan ~ 0.90; He et al., 2011). This suggests that high Th/U in Egongbao and Yunfengding must be produced by processes after zircon crystallization, e.g., fluid exsolution/dehydration after solidification. No correlation between $\delta^{56}Fe$ and Th/U has been found for Dabie non-adakitic granitoids and LMA, with the most fractionated samples in the context of $\delta^{56}Fe$ having typical LCC Th/U. This suggests that fluid exsolution played a negligible role in the origin of the variable $\delta^{56}Fe$ observed in these samples.

In the following, we assess the role of fractional crystallization, source heterogeneity, partial melting and melt-mantle interaction on the origin of $\delta^{56}Fe$ variations in non-adakitic granitoids, LMA and HMA.

5.1. Origin of the $\delta^{56}Fe$ variation in Dabie non-adakitic granitoids

$\delta^{56}Fe$ of Dabie non-adakitic granitoids increase with increasing SiO_2 and $Fe^{3+}/\Sigma Fe$ and decreasing FeOt, MgO, and Mg# (Figs. 2 and 4), suggesting a possible role of fractional crystallization. The Dabie I-type non-adakitic granitoid trend can be modelled with a fractionation factor of $\Delta^{56}Fe_{\text{melt-crystal}} \sim 0.06‰$ using the Rayleigh equation:

$$\delta^{56}Fe_{melt} = \delta^{56}Fe_{melt0} - \Delta^{56}Fe_{melt-crystal} \times \ln(f_{Fe}) \quad (1)$$

where f_{Fe} represents the Fe fraction in the remaining melt (Fig. 4a). Fe isotope fractionation during fractional crystallization is controlled by the ratio of Fe^{3+}-rich oxides to Fe^{2+}-rich minerals in the crystallizing phases and the magma composition. Since Fe^{3+}-O bonds is typically stronger than Fe^{2+}-O bonds both in silicates and in oxides (Dauphas et al., 2014; Roskosz et al., 2015; Sossi and O'Neill, 2017), crystallization of Fe^{2+}-rich silicate and oxide minerals tends to increase $\delta^{56}Fe$ of the evolving melt, while crystallization of Fe^{3+}-rich magnetite tends to decrease $\delta^{56}Fe$ of the evolving melt (Sossi et al., 2012; Foden et al., 2015). $\Delta^{56}Fe_{melt-crystal} \sim 0.06‰$ thus indicates fractional crystallization with Fe^{2+}-rich silicate and oxide minerals as the dominant crystallizing Fe-bearing phases, which is supported by petrological observations (He et al., 2011) and can also explain the correlations between $\delta^{56}Fe$ and Mg#, $Fe^{3+}/\Sigma Fe$ defined by the Dabie I-type non-adakitic granitoids. Clinopyroxene, amphibole, and biotite are the major mafic minerals in Dabie I-type non-adakitic granitoids with accessory magnetite (He et al., 2011). Therefore, the $\delta^{56}Fe$ variation in Dabie I-type non-adakitic granitoids can be explained by fractional crystal-

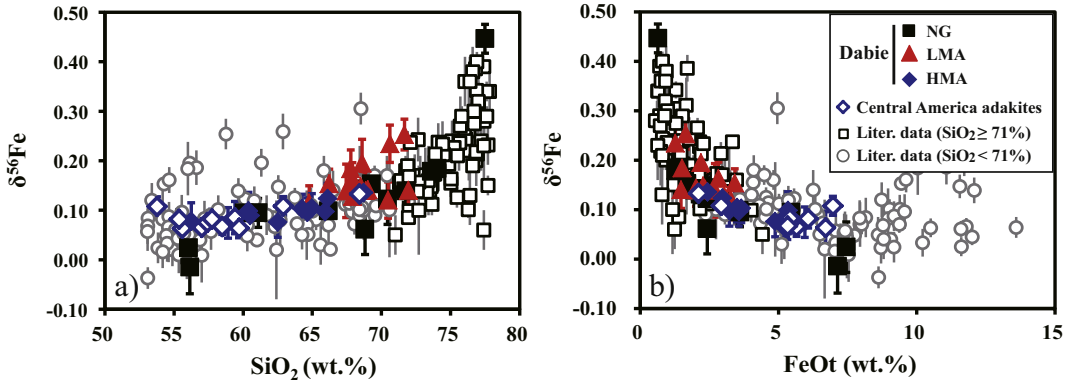

Fig. 2. Evolution of iron isotopic composition with SiO_2 (a) and FeOt (b) for intermediate to felsic igneous rocks (SiO_2 > 53 wt.%). Literature data are from Dauphas et al. (2009a), Heimann et al. (2008), Poitrasson and Freydier (2005), Schuessler et al. (2009), Sossi et al. (2012), Telus et al. (2012), Zambardi et al. (2014) and Foden et al. (2015).

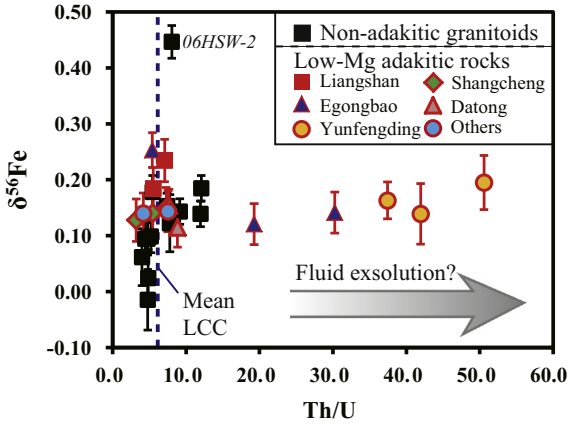

Fig. 3. $\delta^{56}Fe$ vs Th/U diagram for Dabie non-adakitic rocks and LMA. Data source are referred to Fig.2.

lization. Rhyolite-MELTS is not adopted here to model the fractional crystallization process, due to its shortage to calculate hydrous mafic silicates, particularly amphibole and biotite (Gualda et al., 2012; see Appendix for details).

Sample 06HSW-2, which has an affinity to A-type granites (Fig. S3), is plotted off the Dabie I-type non-adakitic granitoid trends by its higher $\delta^{56}Fe$ up to 0.447‰ at given FeOt and $Fe^{3+}/\Sigma Fe$. This supports the previous conclusion that enrichment of heavy Fe is favored in A-type granites (Foden et al., 2015). A-type granites can be produced by extensive differentiation of basaltic magma (Turner et al., 1992). By assuming an arbitrary MORB-like parental magma, an integrated $\Delta^{56}Fe_{melt\text{-}crystal} \sim 0.13‰$ is needed to explain the high $\delta^{56}Fe$ of 06HSW-2. Here we explain this higher $\Delta^{56}Fe_{melt\text{-}crystal}$, compared to what is necessary for the I-type samples, after Dauphas et al. (2014) and Foden et al. (2015). On the one hand, the parental magma of 06HSW-2 likely differentiated with a less extent of integrated magnetite crystallization (Foden et al., 2015). On the other hand, abundant alkaline cations in 06HSW-2 tend to stabilize melt Fe^{2+} and Fe^{3+} in low coordinations, increasing the fractionation factor of the melt and producing a larger $\Delta^{56}Fe_{melt\text{-}crystal}$ (Schuessler et al., 2009; Dauphas et al., 2014; Foden et al., 2015). Alkalis (Na and K) have the potential to stabilize Fe^{3+} in tetrahedral coordination, while alkaline earth cations (Ca and Mg) tend to stabilize Fe^{3+} in octahedral coordination due to their different ionisation potential and ability to balance the charge of $^{IV}Fe^{3+}$–O bonds (Mysen et al., 1980; Galoisy et al., 2001). Meanwhile, the average coordinated number of Fe^{2+} in glasses decreases from 5.2 to 4.5 corresponding to increasing (Na + K)/(Mg + Ca) from 0.3 to 6.1 (Jackson et al., 2005). This magma compositional control on Fe isotope fractionation has been previously indexed by (Na + K)/Al (Foden et al., 2015), and here we suggest (Na + K)/(Ca + Mg) as a better index for the counteracting role of alkaline and alkaline-earth cations (Fig. 5). Positive correlations between $\delta^{56}Fe$ and (Na + K)/Al, (Na + K)/(Ca + Mg) have been observed for most currently available data for high silica ($SiO_2 \geqslant 71$ wt.%) granitic samples, e.g., $\delta^{56}Fe = 0.0062‰ \times (Na + K)/(Ca + Mg) + 0.130‰$ ($R^2 = 0.66$) (Fig. 5). It should be noted that both (Na + K)/Al and (Na + K)/(Ca + Mg) of the melt increase during fractional crystallization until when K-feldspar is dominant (Appendix). The positive correlation between $\delta^{56}Fe$ and (Na + K)/(Ca + Mg) is in part due to fractional crystallization of mafic minerals. If we accept that fractional crystallization of Fe^{2+}-rich silicate and oxide minerals dominates during the formation of A-type granites (Foden et al., 2015), since which tends to increase melt $\delta^{56}Fe$ irrespective of magma composition, this correlation can serve as the maximum estimate of the magma compositional control on Fe isotope fractionation.

A-type granites have been also controversially explained by partial melting of water-poor, melt-depleted source rocks (Whalen et al., 1987). Their alkaline enrichment can be explained by the low degree of partial melting, breakdown of residual micas, and the presence of residual calcic plagioclase (Clemens et al., 1986; Whalen et al., 1987). In this case, the $\delta^{56}Fe$ difference between A-type granites and I- and S-type ones must reflect the difference in Fe isotope fractionation during crustal melting. According to the discussion above, $\Delta^{56}Fe_{melt\text{-}residue}$ during partial melting for

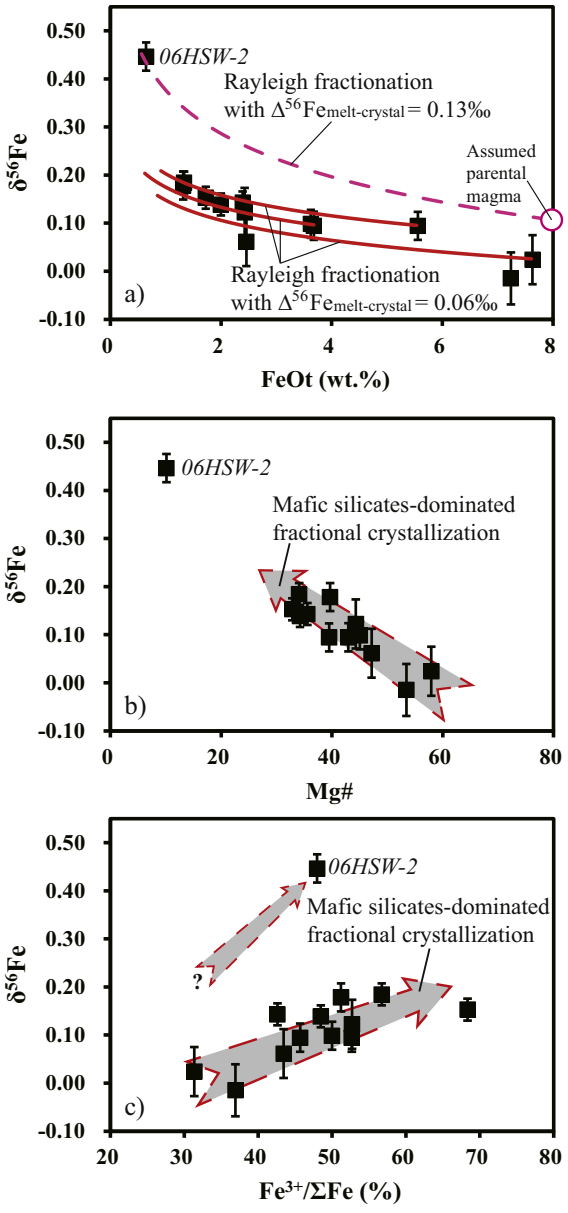

Fig. 4. δ^{56}Fe vs FeOt (a), MgO (b), and $Fe^{3+}/\Sigma Fe$ (c) for Dabie non-adakitic granitoids. Fractionation lines in (a) are calculated using the Rayleigh equation.

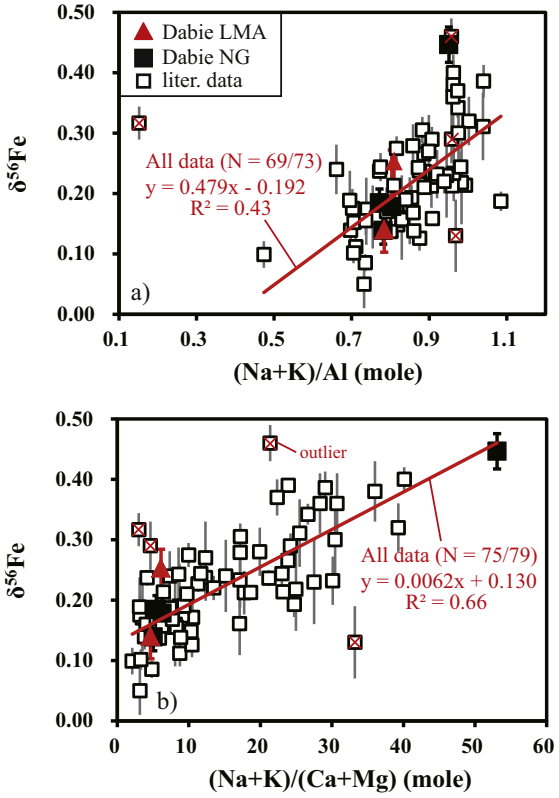

Fig. 5. δ^{56}Fe vs (Na + K)/Al (a) and (Na + K)/(Ca + Mg) (b) for currently available data for high silica ($SiO_2 \geqslant 71$ wt.%) granitic magmas. Literature data sources are same to Fig.2.

A-type granites is expected to be larger than that for I- and S-type granites due to the higher (Na + K)/(Ca + Mg) of the former, and may account for the preference of high δ^{56}Fe in A-type granites. The force constants recently measured for basaltic to rhyolitic glasses (Dauphas et al., 2014), however, predict $10^3\ln\beta_{melt}$ of high (Na + K)/(Mg + Ca) (>135) rhyolitic melts only higher than that of low (Na + K)/(Mg + Ca) (<1) basaltic to dacitic ones by $\leqslant$0.10‰ at temperature $\geqslant$800 °C. If $10^3\ln\beta_{residue}$ keeps constant, this can only explain $\leqslant$1/3 of the δ^{56}Fe variation currently observed in high silica granitic samples (Fig. 5). Therefore, δ^{56}Fe data do not support partial melting of water-poor, melt-depleted source rocks as a common origin of A-type granites, unless i) there is evidence showing that the sources of A-type granites have δ^{56}Fe higher than those of I- and S-type ones; and ii) future experimental calibration suggests a stronger magma compositional control than the theoretical prediction based on the mean force constants of Fe-O bonds (see the discussion in Section 5.3).

5.2. Subtle residual garnet effect observed in Dabie low-Mg adakitic rocks

Dabie LMA were likely derived from low degree eclogitic partial melting with two dominant residual minerals, garnet and clinopyroxene (He et al., 2011), which provides the potential to reveal the effect of source mineralogy on δ^{56}Fe of partial melts. 14 out of 15 Dabie LMA samples indeed yield a positive correlation between δ^{56}Fe and $(Dy/Yb)_N$ (Fig. 6a). Before evaluating the independent effect of source mineralogy, it is necessary to access to what extent magma differentiation and/or source heterogeneity may contribute to the observed δ^{56}Fe variation in Dabie LMA. Significant Fe isotope fractionation due to magma differentiation is not evident for most Dabie LMA, except for EGB-7, based on the following observations: (i) samples from the same pluton generally have identical δ^{56}Fe, irrespective of their variable MgO and FeOt (Fig. 7); (ii) $(Dy/Yb)_N$ does not correlate with SiO_2 (He et al., 2011); (iii) crystallization of amphibole and biotite, the only mafic minerals present in LMA (Wang et al., 2007; He et al., 2011), tends to increase δ^{56}Fe but simultaneously decrease

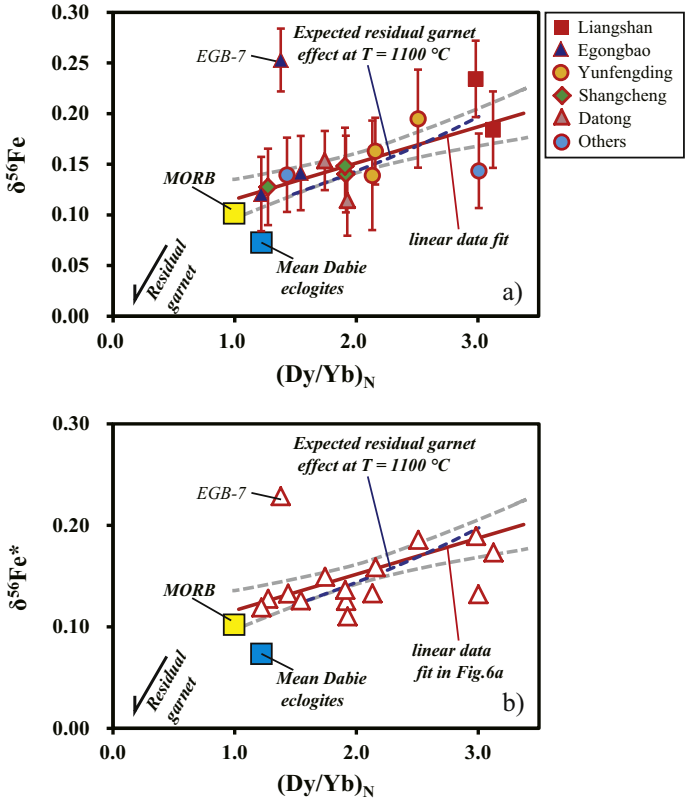

Fig. 6. $\delta^{56}Fe$ vs $(Dy/Yb)_N$ for Dabie low-Mg adakitic rocks (a). A linear fitting to the data yields: $y = (0.0343 \pm 0.016) * x + (0.083 \pm 0.034)$, MSWD = 1.6; shown as the red solid line with gray ones enveloping the 2σ space of the regression. EGB-7 (0.253‰, 1.4), not shown in this figure, is plotted off the trend, likely due to late stage differentiation. The predicted residual garnet effect (the blue dashed line) is calculated using the parameters listed in Table 2. $\delta^{56}Fe^*$ of Dabie LMA, corrected for possible maximum magma compositional control according to the trend in Fig. 5b, is also plotted against $(Dy/Yb)_N$ for comparison (b). (For interpretation of the references to colour in this figure legend, the reader is referred to the web version of this article.)

$(Dy/Yb)_N$ of the melt (GERM; Schuessler et al., 2009; Telus et al., 2012), and would counteract the positive correlation between $\delta^{56}Fe$ and $(Dy/Yb)_N$ observed for most Dabie LMA. LMA sample EGB-7 plots off the major LMA trend in Fig. 6 due to its enhanced $\delta^{56}Fe$ up to 0.253‰ at a given $(Dy/Yb)_N$, which is also higher than the other two samples ($\delta^{56}Fe \sim 0.13$‰) from the same locality (Fig. 7). EGB-7 has a low FeOt content (1.65 wt.%) with negative Eu anomaly ($Eu^* = 0.89$) when compared with the least differentiated sample from the same pluton (FeOt ~ 3.26 wt.% and $Eu^* \sim 1.24$), indicating that substantial fractional crystallization may occur and enhance the $\delta^{56}Fe$ of EGB-7. $\delta^{56}Fe$ of Dabie LMA do not correlate with $^{87}Sr/^{86}Sr_i$ and $\varepsilon_{Nd}(t)$ (Fig. 8), indicating that their sources may have similar Fe isotopic compositions. In addition, high $(Dy/Yb)_N$ of Dabie LMA was attributed to presence of abundant residual garnet in their sources during partial melting (He et al., 2011). The positive correlation between $\delta^{56}Fe$ and $(Dy/Yb)_N$ observed in Dabie LMA, thus, most likely reflects the difference in isotope fractionation scale during crustal melting, and indicates a subtle but detectable residual garnet effect.

It is not clear whether the magma compositional control also contributes to $\delta^{56}Fe$ of the Dabie LMA, given that most (13/15) of them have $SiO_2 < 71$ wt.%. The small range of (Na + K)/(Ca + Mg) (2.3 ~ 9.4) and the slope in Fig. 5b suggest that the magma compositional control on $\delta^{56}Fe$ of the Dabie LMA, if applicable, could be too small to be significant (<0.045‰) (Fig. 6b).

The Dabie LMA trend is compared with the residual garnet effect predicted for eclogitic partial melting based on available $\Delta^{56}Fe_{garnet\text{-}cpx}$ (Fig. 6a). $(La/Yb)_N$ of Dabie LMA are sensitive to the degree of partial melting, because of the incompatibility of La. High $(La/Yb)_N$ at given $(Dy/Yb)_N$ up to 152 suggest a low degree (~5%) of partial melting (He et al., 2011). At a low degree of partial melting, $(Dy/Yb)_N$ of Dabie LMA, varying from 1.2 to 3.1, are mainly determined by D_{Dy}/D_{Yb}, reflecting residual garnet abundance in their sources from 5% to 30% (He et al., 2011; Appendix). To reconcile the correlation between $\delta^{56}Fe$ and $(Dy/Yb)_N$ observed in Dabie LMA, $(Dy/Yb)_N$ of partial melts from a mean continental lower crust source are calculated using the batch partial melting model (Shaw, 1970) and parameters listed in Table 2. Given the definition of $\Delta^{56}Fe$, $\delta^{56}Fe$ of partial melts can be written as:

$$\delta^{56}Fe_{melt} = \Delta^{56}Fe_{melt-residue} + \delta^{56}Fe_{residue} \quad (2)$$

Considering the low FeOt contents of Dabie LMA compared to their sources (Table S3), low degree eclogitic partial melting should have a negligible effect on the Fe

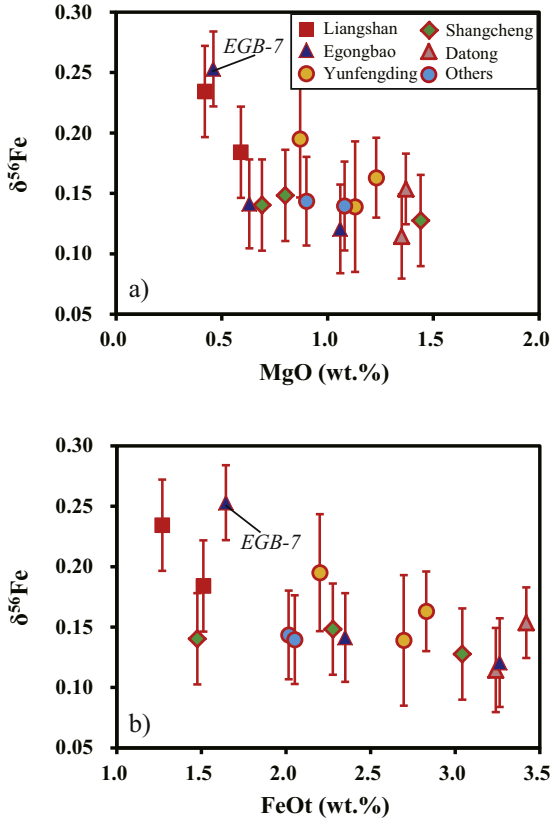

Fig. 7. $\delta^{56}Fe$ vs MgO (a) and FeOt (b) for Dabie low-Mg adakitic rocks. Elemental data are from Wang et al. (2007) and He et al. (2011).

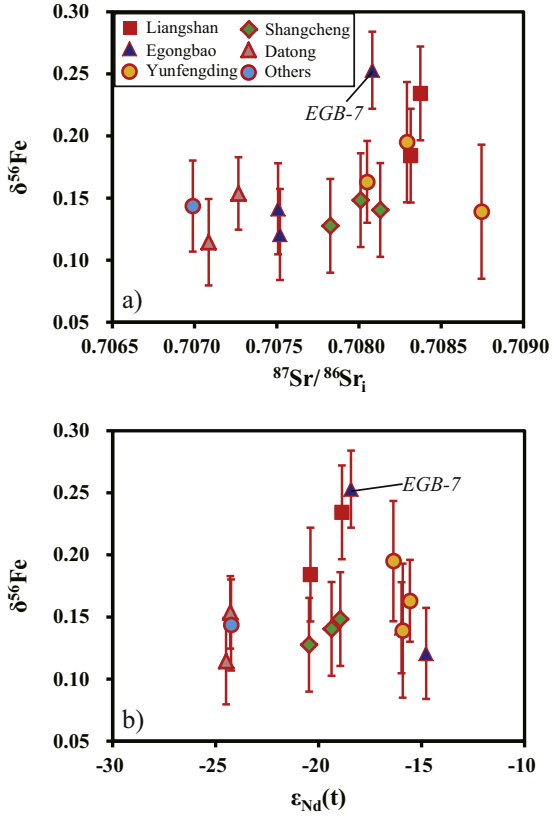

Fig. 8. $\delta^{56}Fe$ vs $^{87}Sr/^{86}Sr_i$ (a) and $\varepsilon_{Nd}(t)$ (b) for Dabie low-Mg adakitic rocks.Sr-Nd isotopic data are from Wang et al. (2007) and He et al. (2013).

isotopic composition of the residual sources. Eq. (2) can be approximated by:

$$\delta^{56}Fe_{melt} = \Delta^{56}Fe_{melt-residue} + \delta^{56}Fe_{source} \quad (3)$$

In addition, $\Delta^{56}Fe_{melt\text{-}residue}$ can be calculated by a Fe fraction weighted average of $\Delta^{56}Fe_{melt\text{-}garnet}$ and $\Delta^{56}Fe_{melt\text{-}cpx}$.

$$\Delta^{56}Fe_{melt-residue} = f_{Fe,garnet} \times \Delta^{56}Fe_{melt-garnet} + (1 - f_{Fe,garnet}) \times \Delta^{56}Fe_{melt-cpx} \quad (4)$$

which can be reduced into:

$$\Delta^{56}Fe_{melt-residue} = \Delta^{56}Fe_{melt-cpx} - f_{Fe,garnet} \times \Delta^{56}Fe_{garnet-cpx} \quad (5)$$

Combined Eqs. (3) and (5), then,

$$\delta^{56}Fe_{melt} = \delta^{56}Fe_{source} + \Delta^{56}Fe_{melt-cpx} - f_{Fe,garnet} \times \Delta^{56}Fe_{garnet-cpx} \quad (6)$$

where $f_{Fe,garnet} = \frac{D_{garnet/cpx}(FeOt) \times A_{garnet}}{A_{cpx} + D_{garnet/cpx}(FeOt) \times A_{garnet}}$, and A_{garnet} represents the garnet abundance in the residue. $D_{garnet/cpx}$ (FeOt) is calculated from experimental residua of Rapp and Watson (1995). The mean $\Delta^{56}Fe_{garnet\text{-}cpx}$ measured in natural samples ($\sim -0.38 \times 10^6/T^2$; Beard and Johnson, 2004; Williams et al., 2009; Williams and Bizimis, 2014) is larger than what is predicted by Sossi and O'Neill (2017) ($\sim -0.18 \times 10^6/T^2$) based on Fe–O bonding data of pure almandine. This discrepancy could be attributed to the possible garnet compositional control on $\Delta^{56}Fe_{garnet\text{-}cpx}$ (Fig. S6 and see Appendix for details). The residual garnet during eclogitic partial melting could be more similar to the counterpart in natural eclogites in composition. Therefore, here we adopt the mean $\Delta^{56}Fe_{garnet\text{-}cpx}$ observed in natural samples in the modelling. As shown in Fig. S7, the choice of $\Delta^{56}Fe_{garnet\text{-}cpx}$ is not important for the explanation of the correlation between $\delta^{56}Fe$ and $(Dy/Yb)_N$ observed in Dabie LMA, as a result of residual garnet effect. Initial magma temperature of Dabie LMA is probably >1075 °C (Xiao and Clemens, 2007). At 1100 °C, increase of the residual garnet proportion from 5% to 30% can increase $\delta^{56}Fe_{melt}$ by ca. 0.076‰ if all else keep constant (Table 2). The mean $\delta^{56}Fe$ of local eclogites (~0.07‰; Zhu et al., 2015b) is taken to approximate the source composition. $\Delta^{56}Fe_{melt\text{-}cpx} \sim 0.03$‰ is adopted to fit the observed LMA trend. This value could be reasonable, given the absence of any equilibrium Fe isotope fractionation between clinopyroxene and its basaltic host (Weyer and Seitz, 2012) and that Dabie LMA melts with $SiO_2 \sim 69$ wt.% may have $10^3 ln\beta_{melt}$ slightly higher than that of basalt (Dauphas et al., 2014). The observed correlation between $\delta^{56}Fe$ and $(Dy/Yb)_N$ in Dabie LMA is perfectly consistent with what is predicted for eclogitic partial melting with residual garnet abundance varying from 5% to 30% (Fig. 6a), indicating that residual

Table 2
Parameters adopted and modelling results for eclogitic partial melting.

	Source composition	Partition coefficient	
		Garnet	Cpx
FeOt	11.27%	$D_{grt/cpx}$ (FeOt) = 2.17	
$\delta^{56}Fe$	0.071‰	$\Delta^{56}Fe_{grt\text{-}cpx} = -0.202‰$, $\Delta^{56}Fe_{melt\text{-}cpx} = 0.028‰$	
Dy	3.1	4.4	1.2
Yb	1.5	14	0.9

Predicted melts for 5% degree of eclogitic partial melting at 1100°C

Source mineralogy	$f_{Fe,\ grt}$	$\Delta^{56}Fe_{melt\text{-}residue}$	$\delta^{56}Fe_{melt}$	$(Dy/Yb)_N$
5% grt + 95% cpx	0.10	0.049‰	0.120‰	1.5
10% grt + 90% cpx	0.19	0.067‰	0.138‰	1.9
15% grt + 85% cpx	0.28	0.084‰	0.155‰	2.3
20% grt + 80% cpx	0.35	0.099‰	0.170‰	2.6
25% grt + 75% cpx	0.42	0.113‰	0.184‰	2.8
30% grt + 70% cpx	0.48	0.125‰	0.196‰	3.0

Notes: Partition coefficients for garnet and clinopyroxene are from the compilation of He et al. (2011) and Rapp and Watson (1995). Dy and Yb contents of the source of Dabie LMA are assumed to be similar to the mean lower continental crust (Rudnick and Gao, 2003). Fe isotopic data for lower continental crust is still lacking. Mean FeOt and $\delta^{56}Fe$ of Dabie eclogites are adopted here to approximate the source of Dabie LMA. $(Dy/Yb)_N$ and $\delta^{56}Fe$ of predicted melts are calculated based on the batch melting model (Shaw, 1970) and equations listed in the main text.

mineralogy may play an important role in fractionating Fe isotopes during eclogitic partial melting.

5.3. Homogeneous Fe isotopic compositions in high-Mg adakites

Dabie and Central America high-Mg adakites have quite homogeneous Fe isotopic compositions with mean $\delta^{56}Fe$ as $0.098 \pm 0.038‰$ (2SD, $N = 11$) and $0.085 \pm 0.045‰$ (2SD, $N = 11$) respectively. This is consistent with the petrogenesis of the high-Mg adakites. These magmas were originally derived from eclogitic partial melting of Dabie lower continental crust and the leading edge of the subducted Cocos Ridge and Caribbean large igneous province basement, and must have once suffered melt-mantle interaction based on their high-Mg features (Abratis and Wörner, 2001; He, 2010; Rapp et al., 1999; Huang et al., 2008; Liu et al., 2010; Wegner et al., 2010). Dissolving a considerable mass of peridotite (up to 10% of the melt volume) is required during melt-mantle interaction to explain the higher CaO contents and the diluted adakitic features (e.g., lower Sr/Y, $(Dy/Yb)_N$ and higher Y and Yb contents) of Dabie HMA when compared to LMA (He, 2010). This process should also play a role on modern arc adakites, since only those melts penetrating a hot mantle regime may survive enroute to the surface (Kelemen et al., 2003). The melt-mantle interaction process was modelled using numerical algorithms below and Rhyolite-MELTS to access whether it can explain the MORB-like $\delta^{56}Fe$ of HMA. For each step of calculation, a small fraction (F_{DM}) of depleted mantle (DM) peridotite (Salters and Stracke, 2004) was added into the hybridizing melt:

$$C_{sys} = (1 - F_{DM}) \times C_{melt0} + F_{DM} \times C_{DM} \quad (7)$$

$$\delta^{56}Fe_{sys} = (1 - f_{Fe,DM}) \times \delta^{56}Fe_{melt0} + f_{Fe,DM} \times \delta^{56}Fe_{DM}, \quad (8)$$

where $f_{Fe,\ DM}$ represents the Fe fraction of assimilated DM peridotite in the system:

$$f_{Fe,DM} = \frac{F_{DM} \times C_{DM}}{(1 - F_{DM}) \times C_{melt0} + F_{DM} \times C_{DM}} \quad (9)$$

Then the magma system was equilibrated at selected temperature and pressure using Rhyolite-MELTS (Gualda et al., 2012; Gualda and Ghiorso, 2015), which provides fractions and elemental compositions of the co-existing melt and crystals. $\delta^{56}Fe$ of the resulting melt was calculated according to mass balance:

$$\delta^{56}Fe_{melt1} = \delta^{56}Fe_{sys} + f_{Fe,crystal} \times \Delta^{56}Fe_{melt-crystal} \quad (10)$$

where $f_{Fe,crystal} = F_{crystal} \times \frac{C_{crystal}}{C_{sys}}$, representing the Fe fraction in the crystals. The calculation was repeated 150 times with the C_{melt1} and $\delta^{56}Fe_{melt1}$ of each step as the initial compositions of the next. Pristine adakitic melts are represented by 06LS-2 and EGB-7, to reflect possible variations in melt composition, and are assumed to react with the upper mantle at 15 kbar, a pressure typical at the crust-mantle boundary. Temperature varies from that of the ambient mantle (~1300 °C) to 1200 °C. The oxygen fugacity is buffered at QFM + 2.5. Other parameters adopted for the modelling are listed in Table 3. The modelling typically reveals two stages of reaction: (i) dissolution of the mantle peridotite due to the high temperature (>the liquidus of the hybridizing melt); (ii) melt0 + peridotite −> melt1 + orthopyroxene, consistent with what is predicted by Kelemen et al. (2003) and observed in Rapp et al. (1999). The hybridizing melt tends to reach a similar $\delta^{56}Fe \sim 0.05‰$, largely determined by $\delta^{56}Fe_{DM} + \Delta^{56}Fe_{melt\text{-}crystal}$, irrespective of the other conditions. This may explain why HMA measured here have almost the same $\delta^{56}Fe$. $\delta^{56}Fe$ of the calculated hybridizing melt, however, is lower than the mean value of HMA. A similar inconsistency has been also found between the predicted MORB and the observed one, and

Table 3
Parameters adopted in this study for modelling of melt-mantle interaction using Rhyolite-MELTS.

Model	Starting composition[#]	Oxygen fugacity buffer	Open/close	P (kbar)	H_2O (wt.%)	T (°C)	Initial $\delta^{56}Fe$	Final FeOt (wt.%)	Final $\delta^{56}Fe$	Liquid remaining (%)
1	06LS-2	QFM + 2.5	open	15	6.0	1300	0.234	4.53	0.044	99
2	06LS-2	QFM + 2.5	open	15	3.0	1300	0.234	3.14	0.048	99
3	06LS-2	QFM + 2.5	open	15	6.0	1200	0.234	2.90	0.058	88
4	EGB-1	QFM + 2.5	open	15	6.0	1300	0.234	5.22	0.048	99

Notes: Melt-mantle interaction is assumed to occur at high temperatures (1200 ~ 1300 °C) due to heat input from ambient mantle, at 15 kbar, a pressure typical for the crust-mantle boundary, and at QFM + 2.5 buffer. $Fe^{3+}/\Sigma Fe$ data of Dabie HMA suggest their liquidus oxygen fugacity from QFM + 2.2 to QFM + 3.1. 06LS-2 and EGB-1 are selected as the pristine adakitic magmas to represent the diversity of Dabie LMA. Liquidus experiments on Dabie LMA reveal that their pristine magmas likely have $H_2O \sim 6$ wt.% (Xiao and Clemens, 2007). One curve with $H_2O \sim 3$ wt.% was also calculated for comparison. The modelling details are referred to the main text.

may be attributed to uncertainties in the calculated fractionation factors or late isotopic fractionation during magma differentiation (Dauphas et al., 2014; Sossi et al., 2016). Both MORB and HMA are likely not the primary magmas derived from the mantle (e.g., Fig. 9). Accordingly, we suggest that melt-mantle interaction may neutralize the possible $\delta^{56}Fe$ variation in their pristine adakitic melts and make a MORB-like $\delta^{56}Fe$ of high-Mg adakites.

Since iron isotopic data of adakitic rocks are not significantly fractionated from other igneous rocks, the existing upper continental crust $\delta^{56}Fe$ estimate of Foden et al. (2015) ~ 0.10‰ is applicable, even if TTG magmatism was a large contributor to early crust stabilization (e.g., Moyen and Martin, 2012).

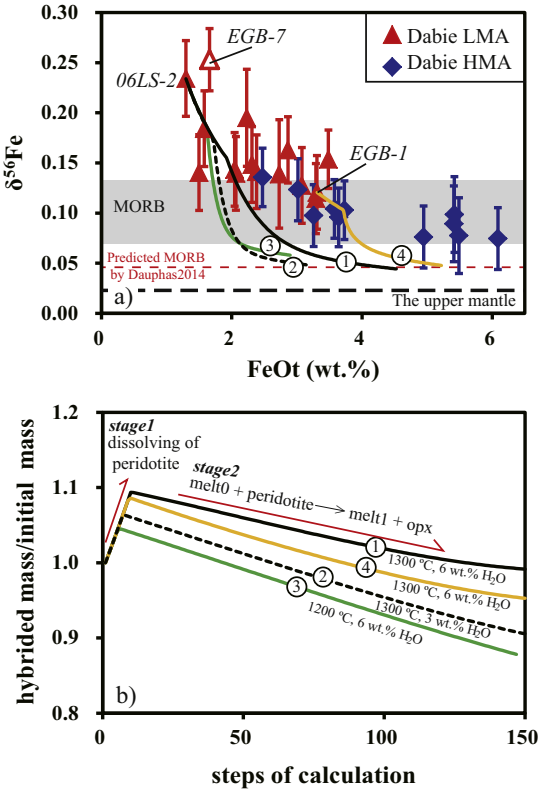

Fig. 9. Iron isotopic fractionation during the melt-mantle interaction that may occur during the formation of high-Mg adakitic rocks. The modelling details are referred to the main text, and the relevant parameters are listed in Table 3.

6. CONCLUSION

To investigate Fe isotope fractionation during intermediate to felsic (especially adakitic) magmatism, we report a comprehensive Fe isotopic data set for adakitic and non-adakitic rocks from the Dabie orogen, central China and typical modern adakites from Central America. The following conclusions can be drawn:

1. I-type Dabie non-adakitic granitoids yield $\delta^{56}Fe$ ranging from −0.015‰ to 0.184‰. The good correlations between $\delta^{56}Fe$ and indices of magma differentiation (e.g., SiO_2, FeOt, Mg#, and $Fe^{3+}/\Sigma Fe$) suggest fractional crystallization with $\Delta^{56}Fe_{melt\text{-}crystal} \sim 0.06$‰ may account for the $\delta^{56}Fe$ variation in these samples.
2. One A-type granite sample from the Dabie orogen has $\delta^{56}Fe$ as high as 0.447‰, which cannot be explained by the same fractional crystallization trends defined by I-type samples but requires higher integrated $\Delta^{56}Fe_{melt\text{-}crystal}$. The necessarily higher $\Delta^{56}Fe_{crystal\text{-}melt} \sim 0.13$‰ may be explained by a decrease in $10^3\ln\beta_{crystal}$ by less magnetite crystallization and an increase in $10^3\ln\beta_{melt}$ due to its high magma (Na + K)/(Ca + Mg). Combined with the literature data, most high silica ($SiO_2 \geqslant 71$ wt.%) granitic rocks define a good positive linear correlation between $\delta^{56}Fe$ and (Na + K)/(Ca + Mg), which can serve as the maximum estimate of the magma compositional control on Fe isotope fractionation.
3. Except for one sample that may have been significantly changed by fractional crystallization, $\delta^{56}Fe$ of Dabie LMA varies from 0.114‰ to 0.234‰ and increases with increasing $(Dy/Yb)_N$. This confirms the prediction that melts derived from eclogitic partial melting with more residual garnet could yield slightly higher $\delta^{56}Fe$.
4. High-Mg adakites from the Dabie orogen and Central America both have homogeneous Fe isotopic compositions with a mean $\delta^{56}Fe \sim 0.10$‰. Melt-mantle interaction processes may neutralize the possible $\delta^{56}Fe$ variation of their pristine adakitic magmas.

ACKNOWLEDGEMENT

Constructive comments from Dr. Paolo Sossi and the two other anonymous reviewers, and efficient handling from Prof. Stefan Weyer are greatly appreciated. We thank Prof. Gerhard Wörner for his kindness providing the Central America adakites and his constructive comments. This work is supported by the DREAM project of Most China (No.2016YFC0600408), the National Natural Science Foundation of China (41473016); the Fundamental Research Funds for the Central Universities (2652014056) and State Key Lab. of Geological Processes and Mineral Resources. This is CUGB petrogeochemical contribution No. PGC-201520.

APPENDIX A.

1. Simplified geological maps and sampling information for Dabie and Central American samples.
2. Classification of Dabie granitoids.
3. Fractional crystallization modelling based on Rhyolite-MELTS.

APPENDIX B. SUPPLEMENTARY DATA

Supplementary data associated with this article can be found, in the online version, at http://dx.doi.org/10.1016/j.gca.2017.01.005.

REFERENCES

Abratis M. and Wörner G. (2001) Ridge collision, slab-window formation, and the flux of Pacific asthenosphere into the Caribbean realm. *Geology* **29**(2), 127–130.

Bali E., Audetat A. and Keppler H. (2009) Mobility of U and Th in subduction zone fluids-A synthetic fluid inclusion study. *Geochim. Cosmochim. Acta* **73**(13), A80.

Beard B. L. and Johnson C. M. (2004) Inter-mineral Fe isotope variations in mantle-derived rocks and implications for the Fe geochemical cycle. *Geochim. Cosmochim. Acta* **68**(22), 4727–4743.

Castillo P. R. (2006) An overview of adakite petrogenesis. *Chin. Sci. Bull.* **51**(3), 258–268.

Clemens J. D., Holloway J. R. and White A. J. R. (1986) Origin of an A-type granite: experimental constraints. *Am. Mineral.* **71**, 317–324.

Craddock P. R. and Dauphas N. (2010) Iron Isotopic Compositions of Geological Reference Materials and Chondrites. *Geostand. Geoanal. Res.* **35**(1), 101–123.

Dauphas N. et al. (2009a) Iron isotopes may reveal the redox conditions of mantle melting from Archean to Present. *Earth Planet. Sci. Lett.* **288**(1–2), 255–267.

Dauphas N., Pourmand A. and Teng F.-Z. (2009b) Routine isotopic analysis of iron by HR-MC-ICPMS: how precise and how accurate? *Chem. Geol.* **267**(3–4), 175–184.

Dauphas N., Roskosz M., Apl E. E., Neuville D. R., Hu M. Y., Sio C. K. and Cordier C. (2014) Magma redox and structural controls on iron isotope variations in Earth's mantle and crust. *Earth Planet. Sci. Lett.* **398**, 127–140.

Defant M. J. and Drummond M. S. (1990) Derivation of some modern arc magmas by melting of young subducted lithosphere. *Nature* **347**(6294), 662–665.

Foden J., Sossi P. A. and Wawryk C. M. (2015) Fe isotopes and the contrasting petrogenesis of A-, I- and S-type granite. *Lithos* **212–215**, 32–44.

Galoisy L., Calas G. and Arrio M. A. (2001) High-resolution XANES spectra of iron in minerals and glasses: structural information from the pre-edge region. *Chem. Geol.* **174**, 307–319.

Gualda G. A. R. and Ghiorso M. S. (2015) MELTS_Excel: a Microsoft Excel-based MELTS interface for research and teaching of magma properties and evolution. *Geochem. Geophys. Geosyst.* **16**, 315–324.

Gualda G. A. R., Ghiorso M. S., Lemons R. V. and Carley T. L. (2012) Rhyolite-MELTS: a modified calibration of MELTS optimized for silica-rich, fluid-bearing magmatic systems. *J. Petrol.* **53**(5), 875–890.

Hawkesworth C. J., Turner S. P., McDermott F., Peate D. W. and vanCalsteren P. (1997) U-Th isotopes in arc magmas: implications for element transfer from the subducted crust. *Science* **276**(5312), 551–555.

He Y. S. (2010) Geochemistry of post-collisional granitic magmatism from the Dabie orogen: constraints on removal processes and architecture of the mountain root. A dissertation for doctor's degree, University of Science and Technology of China (in Chinese with English abstract).

He Y. S., Li S. G., Hoefs J., Huang F., Liu S. A. and Hou Z. H. (2011) Post-collisional granitoids from the Dabie orogen: new evidence for partial melting of a thickened continental crust. *Geochim. Cosmochim. Acta* **75**, 3815–3838.

He Y. S., Li S. G., Hoefs J. and Kleinhanns I. C. (2013) Sr-Nd-Pb isotopic compositions of Early Cretaceous granitoids from the Dabie orogen: constraints on the recycled lower continental crust. *Lithos* **156–159**, 204–217.

He Y. S., Hu D. P. and Zhu C. W. (2015a) Progress of iron isotope geochemistry in geoscience. *Earth Sci. Front.* **22**, 054–071.

He Y. S., Ke S., Teng F. Z., Wang T. T., Wu H. J., Lu Y. H. and Li S. G. (2015b) High-precision iron isotope analysis of geological reference materials by high-resolution MC-ICP-MS. *Geostand. Geoanal. Res.* **39**(3), 341–356.

Heimann A., Beard B. L. and Johnson C. M. (2008) The role of volatile exsolution and sub-solidus fluid/rock interactions in producing high 56Fe/54Fe ratios in siliceous igneous rocks. *Geochim. Cosmochim. Acta* **72**(17), 4379–4396.

Huang F., Li S. G., Dong F., He Y. S. and Chen F. K. (2008) High-Mg adakitic rocks in the Dabie orogen, central China: implications for foundering mechanism of lower continental crust. *Chem. Geol.* **255**(1–2), 1–13.

Jackson W. E., Farges F., Yeager M., Mabrouk P. A., Rossano S., Waychunas G. A. and Brown G. E. (2005) Multi-spectroscopic study of Fe(II) in silicate glasses: implications for the coordination environment of Fe(II) in silicate melts. *Geochim. Cosmochim. Acta* **69**(17), 4315–4332.

Kelemen P. B., Yogodzinski G. M. and Scholl David W. (2003) Along-strike variation in the Aleutian island arc: Genesis of high Mg# andesite and implications for continental crust. *Geophys. Monograp.* **138**, 223–276.

Ling M. X., Wang F. Y., Ding X., Zhou J. B. and Sun W. D. (2011) Different origins of adakites from the Dabie Mountains and the Lower Yangtze River Belt, eastern China: geochemical constraints. *Int. Geol. Rev.* **53**(5–6), 727–740.

Liu S.-A., Li S., He Y. and Huang F. (2010) Geochemical contrasts between early Cretaceous ore-bearing and ore-barren high-Mg adakites in central-eastern China: implications for petrogenesis and Cu–Au mineralization. *Geochim. Cosmochim. Acta* **74**(24), 7160–7178.

Millet M. A., Baker J. A. and Payne C. E. (2012) Ultra-precise stable Fe isotope measurements by high resolution multiple-collector inductively coupled plasma-mass spectrometry with a ^{57}Fe-^{58}Fe double spike. *Chem. Geol.* **304–305**, 18–25.

Moyen J. F. (2009) High Sr/Y and La/Yb ratios: the meaning of the 'adakitic signature'. *Lithos* **112**, 556–574.
Moyen J.-F. and Martin H. (2012) Forty years of TTG research. *Lithos* **148**, 312–336.
Mysen B. O., Seifert F. and Virgo D. (1980) Structure and redox equilibria of iron-bearing silicate melts. *Am. Mineral.* **65**, 867–884.
Poitrasson F. and Freydier R. (2005) Heavy iron isotope composition of granites determined by high resolution MC-ICP-MS. *Chem. Geol.* **222**(1–2), 132–147.
Rapp Watson R. (1995) Dehydration melting of metabasalt at 8–32 kbar: implications for continental growth and crust-mantle recycling. *J. Petrol.* **36**, 891–931.
Rapp R. P., Shimizu N., Norman M. D. and Applegate G. S. (1999) Reaction between slab-derived melts and peridotite in the mantle wedge: experimental constraints at 3.8 GPa. *Chem. Geol.* **160**(4), 335–356.
Roskosz M., Sio C. K. I., Dauphas N., Bi W. L., Tissot F. L. H., Hu M. Y. and Alp E. E. (2015) Spinel–olivine–pyroxene equilibrium iron isotopic fractionation and applications to natural peridotites. *Geochim. Cosmochim. Acta* **169**, 184–199.
Rudnick R. L. and Gao S. (2003). *Composition of the Continental Crust*. In the Crust (ed. R.L. Rudnick) 3 Treatise on Geochemistry (eds. H.D. Holland and K.K. Turekian), Elsevier-Pergamon, Oxford, 1-64.
Salters V. and Stracke A. (2004) Composition of the depleted mantle. *Geochem. Geophys. Geosyst.* **5**(5), 1525–2027.
Schuessler J. A., Schoenberg R. and Sigmarsson O. (2009) Iron and lithium isotope systematics of the Hekla volcano, Iceland - Evidence for Fe isotope fractionation during magma differentiation. *Chem. Geol.* **258**(1–2), 78–91.
Shaw D. M. (1970) Trace element fractionation during anatexis. *Geochim. Cosmochim. Acta* **34**(2), 237–243.
Sossi P. A. and O'Neill C. (2017) The effect of bonding environment on iron isotope fractionation between minerals at high temperature. *Geochim. Cosmochim. Acta* **196**, 121–143.
Sossi P. A., Foden J. D. and Halverson G. P. (2012) Redox-controlled iron isotope fractionation during magmatic differentiation: an example from the Red Hill intrusion, S. Tasmania. *Contribut. Mineral. Petrol.* **164**(5), 757–772.
Sossi P. A., Nebel O. and Foden J. (2016) Iron isotope systematics in planetary reservoirs. *Earth Planet. Sci. Lett.* **452**, 295–308.
Telus M., Dauphas N., Moynier F., Tissot F. L. H., Teng F. Z., Nabelek P. I. and Groat L. A. (2012) Iron, zinc, magnesium and uranium isotopic fractionation during continental crust differentiation: the tale from migmatites, granitoids, and pegmatites. *Geochim. Cosmochim. Acta* **97**, 247–265.
Teng F. Z., Dauphas N. and Helz R. T. (2008) Iron Isotope Fractionation During Magmatic Differentiation in Kilauea Iki Lava Lake. *Science* **320**(5883), 1620–1622.
Teng F.-Z., Dauphas N., Huang S. and Marty B. (2013) Iron isotopic systematics of oceanic basalts. *Geochim. Cosmochim. Acta* **107**, 12–26.
Turner S. P., Foden J. and Morrison R. S. (1992) Derivation of some A-type magmas by fractionation of basaltic magma: an example from the Padthaway Ridge, South Australia. *Lithos* **28**, 151–179.
Wang Q., Wyman D. A., Xu J. F., Jian P., Zhao Z. H., Li C. F. and He B. (2007) Early Cretaceous adakitic granites in the Northern Dabie Complex, central China: implications for partial melting and delamination of thickened lower crust. *Geochim. Cosmochim. Acta* **71**(10), 2609–2636.
Wegner W., Wörner G., Harmon R. S. and Jicha B. R. (2010) Magmatic history and evolution of the Central American Land Bridge in Panama since Cretaceous times. *Geol. Soc. Am. Bull.* **123**(3–4), 703–724.
Weyer S. and Ionov D. A. (2007) Partial melting and melt percolation in the mantle: the message from Fe isotopes. *Earth Planet. Sci. Lett.* **259**(1–2), 119–133.
Weyer S. and Seitz H. M. (2012) Coupled lithium- and iron isotope fractionation during magmatic differentiation. *Chem. Geol.* **294–295**, 42–50.
Whalen J. B., Currie K. L. and Chappell B. W. (1987) A-type granites: geochemical characteristics, discrimination and petrogenesis. *Contrib. Miner. Petrol.* **95**, 407–419.
Williams H. M. and Bizimis M. (2014) Iron isotope tracing of mantle heterogeneity within the source regions of oceanic basalts. *Earth Planet. Sci. Lett.* **404**, 396–407.
Williams H. M., Nielsen S. G., Renac C., Griffin W., O'Reilly S. Y., McCammon C. A. and Halliday A. N. (2009) Fractionation of oxygen and iron isotopes by partial melting processes: implications for the interpretation of stable isotope signatures in mafic rocks. *Earth Planet. Sci. Lett.* **283**(1–4), 156–166.
Xiao L. and Clemens J. D. (2007) Origin of potassic (C-type) adakite magmas: experimental and field constraints. *Lithos* **95**(3–4), 399–414.
Yin M., and Li J. X. (2011) Analysis of Rock and Minerals. Geological Publishing House, Beijing, vol. 2, pp.1–862 (in Chinese)
Zambardi T., Lundstrom C. C., Li X. X. and McCurry M. (2014) Fe and Si isotope variations at Cedar Butte volcano: insight into magmatic differentiation. *Earth Planet. Sci. Lett.* **405**, 169–179.
Zhu D., Bao H. M. and Liu Y. (2015a) Non-traditional stable isotope behaviors in immiscible silica-melts in a mafic magma chamber. *Sci. Rep.* **5**, 17561.
Zhu C. W., He Y. S., Wu H. J. and Li S. G. (2015b) Iron isotope fractionation behavior during subduction metamorphism: an example from the Dabie-Sulu orogen. *J. Jilin Univ. (Earth Science Edition)* **45**(Suppl. 1), 1520–1523.

Associate editor: Stefan Weyer